RESEARCH COMMUNICATION

Disrupted Surfaces of Porous Membranes Reduce Nuclear YAP Localization through Diminished Cell Spreading and Enhance Adipogenesis

Zahra Allahyari†,‡, Stephanie M. Casillo‡, Spencer J. Perry‡, Ana P. Peredo‡, Shayan Gholizadeh†,‡ and Thomas R. Gaborski‡

† Department of Microsystems Engineering, Rochester Institute of Technology, 160 Lomb Memorial Drive, Rochester, NY 14623, USA

‡ Department of Biomedical Engineering, Rochester Institute of Technology, 160 Lomb Memorial Drive, Rochester, NY 14623, USA

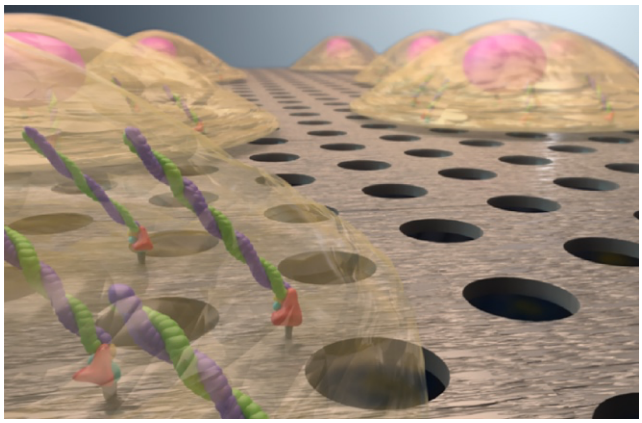

ABSTRACT

Downstream effects of cell-substrate interactions due to porous membranes are not fully understood. Consistent with previous studies using other types of discontinuous or disrupted substrates, we show adipose-derived stromal cells cultured on porous membranes have reduced spreading and nuclear YAP localization as well as an increased propensity towards adipogenesis.

CORRESPONDING AUTHOR:
* e-mail: tom.gaborski@rit.edu; twitter: @tomgaborski; ORCID: 0000-0002-3676-3208

KEYWORDS: Mechanotransduction, Membranes, Differentiation, YAP

There is a growing interest in disrupted substrates in the form of porous membranes, microposts, and micropillars in tissue engineering applications and stem cell studies due to their ability to tailor and recapitulate a physiologically relevant microenvironment.[1–10] Microposts and micropillars are widely used for their controllable mechanical properties in biomimicking cellular microenvironments and providing mechanical cues.[7–9] Porous membranes can enable physiologically relevant cell-cell communication between co-cultured cells and are widely used in developing organ-on-a-chip and barrier models.[1–6,11] Furthermore, there have been several informative studies investigating the role of nano and micro topography in cell-substrate interaction and mechanotransduction.[12–15] However, the results from these studies are rarely applied or considered when using porous membranes in cell culture or tissue-on-a-chip devices. This issue is most apparent with microporous membranes applications where membranes are used as a semi-permeable transmigration barrier or to compartmentalize different cell types, but not to intentionally modify or perturb cell-substrate interactions. The role of surface discontinuity on cellular behavior of vascular endothelial cells was previously explored by our group, and it was demonstrated that membrane pores can alter fibronectin fibrillogenesis and cell migration, as well as F-actin polymerization, and focal adhesion (FA) formation.[16,17] In another study, we showed that many of the observed changes in cellular behaviors over porous membranes could also be replicated by non-fouling micro-patterns which resemble membrane pores with regular disruption in cell-substrate interaction.[18] These results suggest that surface disruption is responsible for the reduced weakened cell-substrate interaction and downstream effects.

Mechanotransduction is the mechanism by which cells sense and respond to the mechanical forces and physical properties of their microenvironment. The effects of these mechanical cues can drive cell differentiation, determine cell fate, and define tissue architecture.[19] Yes-associated protein (YAP) is a major transcriptional coactivator and a hippo pathway effector that mediates mechanotransduction while activated by localization to nuclei.[20,21] YAP localization and activation are strongly correlated with substrate stiffness,[19,22–25] and it has been shown that YAP can direct mesenchymal stem cell fate toward an osteogenic lineage on stiffer substrates.[22,26] Although our previous efforts confirmed the formation of weaker cell-substrate interactions over disrupted substrates, it has not been investigated whether weaker cell-substrate interactions are correlated with altered mechanotransduction signaling pathways, and if they are associated with the YAP nuclear localization and cell fate.

In this study, a rigid non-fouling micropatterned substrate was used to explore how surface disruption might affect cell-substrate interactions and differentiation in mesenchymal cells. The results indicate weakened cell-substrate interaction as well as reductions in YAP nuclear localization on the micropatterned non-fouling substrate, which is similar to the cellular behavior on soft substrates and tissues.[19,27,28] We also confirmed that surface disruption on porous membranes with micron and submicron size pores yielded similar and consistent results. Since there is an increasing interest in utilizing disrupted surfaces in mesenchymal stem cell differentiation, [3,29–31] we also evaluated whether the surface discontinuity of porous membranes could affect stem cell fate.

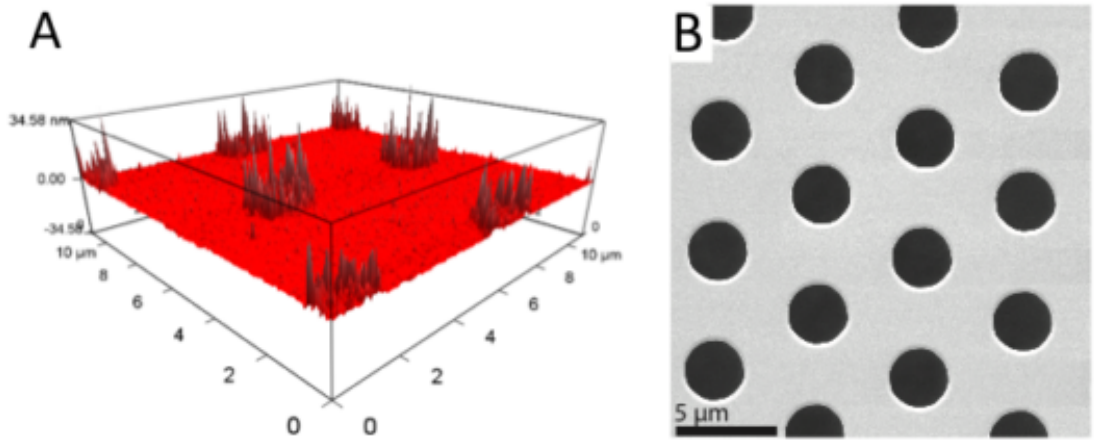

Fig.1. A. Atomic force microscopy of PEG islands on an SiO_2 substrate, **B.** Scanning electron micrographs of SiO_2 membrane with 3.0 µm diameter pores.

The first step for understanding surface disruption-related changes in cell adhesion and mechanotransduction of stem cells was the fabrication of a non-fouling micropattern, which frequently disrupts cell-substrate interaction. The non-fouling micropatterns were developed on a silicon dioxide (SiO_2) layer by combining photolithography and simple polymer adsorption on the surface, described in detail in our previous work.[18] The non-fouling regions were generated using poly(l-lysine)-grafted-poly(ethylene glycol) (PLL-g-PEG). The PLL backbone of the polymer can be adsorbed effectively to any negatively charged substrate, including SiO_2, and the PEG brushes hinder protein adsorption and cell adhesion.[32,33] The non-fouling regions were developed in the form of 3 μm-diameter circles with 6 μm center-to-center spacing in a hexagonal pattern as previously described.[18] Fig. 1A shows the AFM height profile of the PLL-g-PEG-patterned substrate. The unpatterned SiO_2 control substrates were prepared in a similar process but without applying PLL-g-PEG.

The next step after developing a disrupted substrate was to investigate the adhesion and mechanotransduction response of adipose-derived stromal cells (ADSCs) on the disrupted substrates. Mesenchymal cells, including ADSCs, are established models in mechanoresponse and substrate stiffness-related studies.[34–36] We have shown that endothelial cells made weaker adhesion over disrupted substrates in our previous works.[16–18] Here, we first confirmed whether mesenchymal cells also generate weaker interactions due to the substrate discontinuity. Since actin stress fibers are ubiquitous and essential for cell adhesion and mechanosensing,[18,37–39] F-actin content of the ADSCs was evaluated after 24 h of cell seeding (Fig. 2A and B). The method of staining and measurement are explained in the Supplementary Information. The cells showed significantly lower F-actin content on the discontinuous surface of the non-fouling patterned SiO_2 compared to the continuous SiO_2 (Fig. 2C). The diminished F-actin formation on the patterned substrates suggests weakened interaction of ADSCs with the substrates similarly to endothelial cells on porous membranes in our previous studies.[16–18] In the next step, we evaluated FA formation as the most studied and largest adhesion structures in the cells.[14,40] FAs are known to be key players in mechanosensing, and they are considered a bridge between substrate and cytoskeleton.[41–43] FAs were stained and imaged, as explained in the Supplementary Information. There was also a slight but insignificant decrease in the number of distinct FAs over the micropatterned substrates. This result was not entirely consistent with our previous work, where we observed a drastic reduction in FA formation of endothelial cells on disrupted substrates.[16,17] However, we did observe smaller and less elongated FAs over the PEG patterned substrate (Fig. 2A and B). Still, we decided to evaluate another characteristic of cell adhesion. Our next step was to evaluate cell spreading, as another indicator of cell-substrate interaction strength,[38] over PEG patterned and unpatterned substrates after 24 h of cell culture. More than a 30 percent reduction was observed in cell spreading over PEG islands compared to the control SiO_2, which indicates a weaker cell-substrate interaction (Fig. 2G).

After confirming weakened interactions of ADSCs with the disrupted surface of the rigid patterned substrates, which is similar to a cell response to soft substrates, we aimed to investigate mechanotransduction of ADSCs over PEG islands and the unpatterned SiO_2 control substrates to determine whether this mechanism is different over continuous and disrupted substrates of the same stiffnesses. We investigated YAP localization as an indicator of mechanotransduction over these substrates. We measured the nuclear and cytoskeleton YAP content after 6 h and 24 h of cell seeding and calculated the ratio of nuclear to cytoskeletal YAP localization. The method of YAP staining and measuring the nuclear to cytoskeletal YAP ratio can be found in the Supplementary Information. We looked at YAP localization after 6 h of cell seeding and found no significant difference between the control and PEG islands, which was not surprising as the cells were still adhering and spreading on the substrate. After 24 h, however, we observed a statistically significant difference in nuclear YAP localization over the discontinuous PEG micropatterned islands versus the continuous unpatterned SiO_2 control substrates (Fig. 2H). The results indicated that YAP entered the nuclei after ADSCs sensed the stiffness of the rigid continuous SiO_2 substrate. However, the cells did not behave similarly on the patterned SiO_2, and despite the fact that ADSCs were placed on a rigid substrate, the nuclear to cytoskeletal YAP ratio slightly decreased over the PEG islands. These observations demonstrate that the surface disruption and weakened cell-substrate attachment can affect mechanotransduction despite the substrate being extremely stiff such as SiO_2 on a silicon wafer with a Young's modulus >100 GPa. Additionally, this study has confirmed Nardone et al.'s finding where they have shown that YAP nuclear localization can be induced independently of FA formation.[21] They suggested that although YAP can direct FA-related gene expression, FA assembly does not necessarily lead to YAP nuclear localization. It was shown that cell spreading rather than FA assembly regulated YAP localization.[21] Here, we also concluded that cell spreading rather than FA assembly plays the main role in mechanosensing and YAP localization, since we observed a significant decrease in nuclear YAP localization without a significant reduction in FA formation.

We further aimed to confirm the role of surface disruption on mechanotransduction by repeating the experiment on porous membranes since porous membranes are probably the most broadly applied disrupted surfaces in cellular studies.[2,17] To reevaluate mechanotransduction changes on the disrupted substrates, we used ultrathin SiO_2 membranes with an identical pattern to the PEG islands, with two different pore sizes (0.5 or 3 μm), that had been previously developed by our group.[44] These ultrathin (0.3 μm) SiO_2 membranes were hexagonally patterned with a 1:2 pitch (Fig. 1B). The fabricated membranes had approximately 23% porosity and 77% available contact area.[17] The method of fabrication is explained in the Supplementary Information. We seeded ADSCs on the developed porous and non-porous SiO_2 membranes and evaluated

cell spreading and YAP localization after 6 and 24 hours. We found the same trend of reduction in cell spreading and nuclear YAP localization on the porous membranes of both pore sizes as compared to the non-porous SiO_2 membranes. This significant reduction in cell spreading as well as YAP nuclear localization after 24 h confirmed our previous obtained results over PEG patterned substrates and showed that disrupted surfaces of rigid substrates such as patterned SiO_2 could affect mechanotransduction similarly to soft substrates.

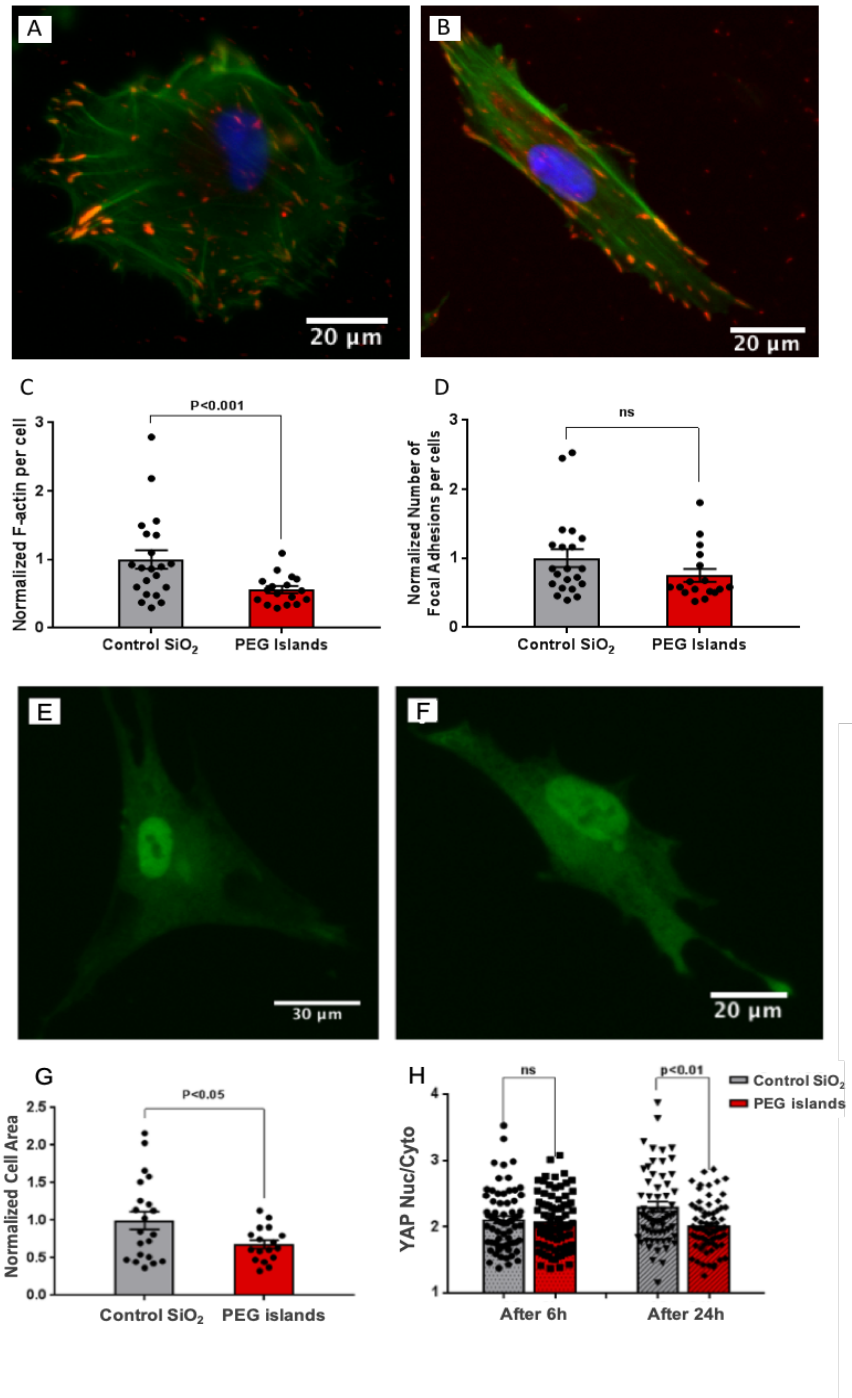

Fig. 2. Fluorescence images of ADSCs stained for F-actin (phalloidin, green), FAs (anti-vinculin, red) and nuclei (DAPI, blue) on (**A**) Control unpatterned SiO_2 substrates and (**B**) SiO_2 substrates with PEG islands after 24 h. (**C**) F-actin intensity per cell normalized to control mean value. (**D**) Distinct FAs per cell normalized to control mean value. Fluorescence images anti-YAP on (**E**) Control unpatterned SiO_2 substrates and (**F**) SiO_2 substrates with PEG islands. (**G**) Cell spread area was quantified from F-actin images. (**H**) YAP nuclear-cytoplasmic ratio is quantified at 6 h and 24 h.

Since there is a growing interest in the application of disrupted surfaces such as porous membranes in co-culture systems for differentiation studies due to their ability to compartmentalize cell culture, [3,29,45–47] we sought to understand whether the altered mechanotransduction over porous membranes could affect cell fate. We aimed to investigate ADSC differentiation into adipocyte and osteocyte lineages on porous and non-porous SiO_2 membranes. ADSCs were seeded on the membranes and fed a 1:1 mixture of adipogenic and osteogenic media for 14 days similar to Guvendiren et al. as explained in the Supplementary Information.[48] We found that cells were more prone to generate lipid vacuoles, indicating adipogenic differentiation,[48,49] over the disrupted substrates of porous membranes after 14 days. On the other hand, far fewer ADSCs expressed lipid vacuoles on the non-porous membranes at the same time point. Instead, the cells over the non-porous

samples expressed more alkaline phosphatase (ALP) than the cells cultured on porous membranes. Since ALP is an enzyme that is highly expressed in the early stage of osteogenesis,[43,50] the enhanced ALP expression in the ADSCs on non-porous membranes shows a preference towards osteogenic differentiation. These results confirmed that mesenchymal stem cell fate is altered on the disrupted substrates compared to continuous substrates. We observed enhanced adipogenic differentiation of mesenchymal cells on the disrupted substrate compared to the continuous substrate, similar to the enhancement on soft substrates versus rigid substrates.[51]

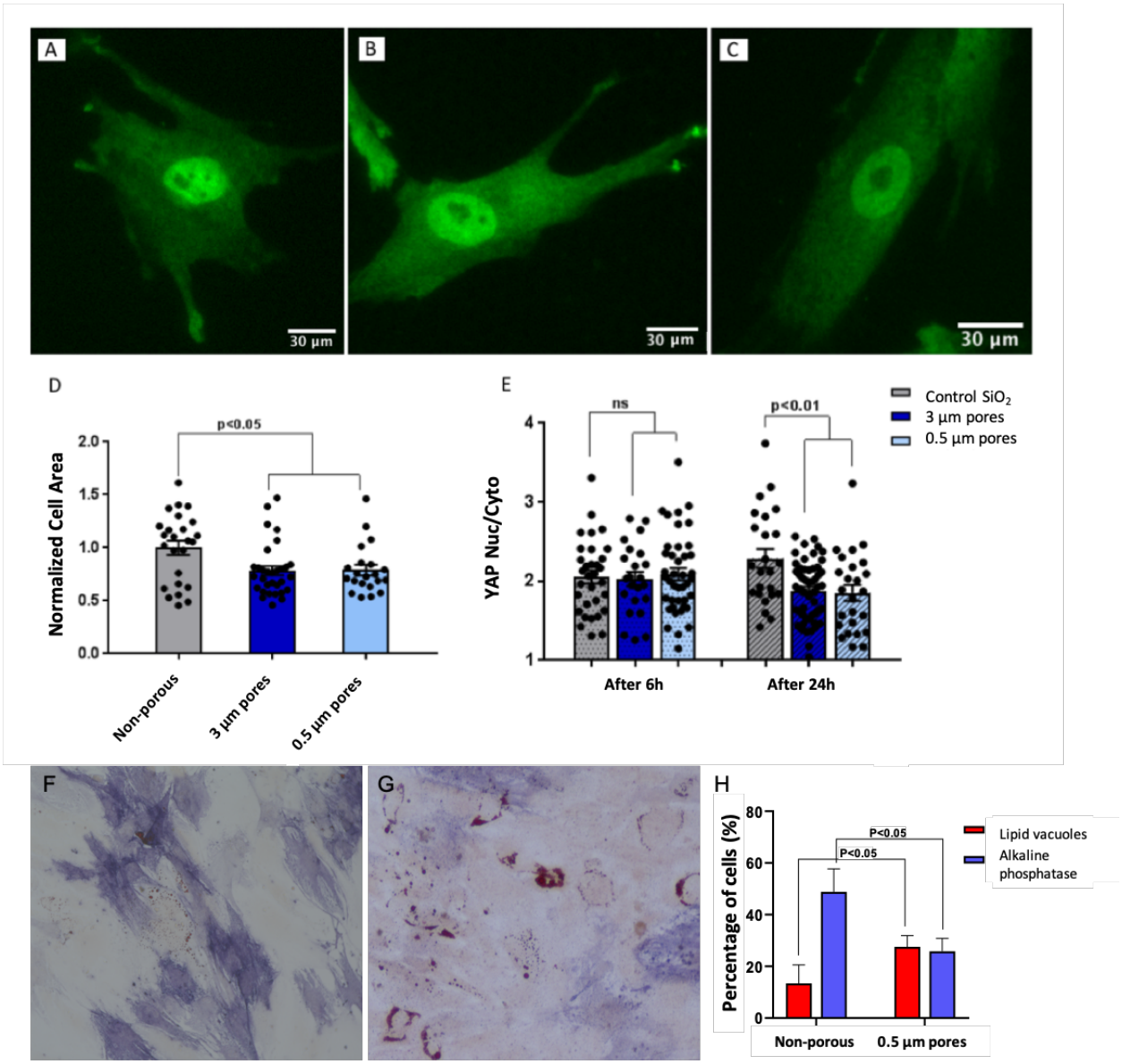

Fig. 3. Fluorescence images ADSCs stained with anti-YAP on (**A**) non-porous, (**B**) 3.0 µm pore diameter and (**C**) 0.5 µm pore diameter SiO_2 membranes after 24 h. (**D**) Cell spread area was quantified from F-actin images at 24 h. (**E**) YAP nuclear-cytoplasmic ratio is quantified at 6 h and 24 h. ADSCs were cultured in mixed adipogenic and osteogenic differentiation media on each substrate for 10 days and then prepared for histological staining. ALP and lipid vacuoles were respectively stained by Fast blue RR and Oil red O on (**F**) non-porous and (**G**) 0.5 µm pore diameter SiO_2 membranes, and (**H**) percentage of the cells expressing lipid vacuoles and alkaline phosphatase which are stained by Oil red O and fast blue RR respectively (n = 4 substrates for each condition; > 400 cells).

CONCLUSION

Our data demonstrate that substrate disruption affects mechanotransduction and stem cell differentiation, where disruption in cell-substrate interaction due to surface discontinuity leads to similar cellular responses as on softer substrates.[19,28,51] Mesenchymal stem cells on discontinuous substrates produce different responses compared to continuous rigid substrates, including weakened cell-substrate interaction, as evidenced by decreased F-actin and cell spreading as well as reduced nuclear YAP localization. These results are consistent on non-fouling micropatterned substrates and porous membranes representing two different types of disrupted substrates. We also looked into the relationship between diminished cell-substrate interaction and mechanotransduction. This work shows that reduced cell spreading rather than FA formation is the potential explanation for reduced nuclear YAP localization. We later confirmed that altered mechanotransduction could lead to different cell fates over the disrupted surfaces. Our finding is consistent with Xia et al., who also demonstrated that surface discontinuity could modulate stem cell differentiation.[43] However, their study was focused on nano-size pores that mimic bone tissue architecture. In contrast, our research is focused on micron-size pores, which are of interest in developing co-culture systems. Our finding demonstrates the importance of surface discontinuity in determining stem cell fate, which should be considered in future differentiation studies that use porous membranes in co-culture platforms to direct tissue and barrier formation.

ACKNOWLEDGEMENTS

We thank Bradley Kwarta for producing the cell-substrate interaction illustrations. The authors declare the following competing financial interest: TRG is a co-founder of SiMPore and has an equity interest in this early-stage company commercializing ultrathin silicon-based technologies.

AUTHOR CONTACT INFORMATION

Thomas R. Gaborski; email: tom.gaborski@rit.edu; twitter: @tomgaborski; ORCID: 0000-0002-3676-3208

AUTHOR CONTRIBUTIONS

The manuscript was written through contributions of all authors. All authors have given approval to the final version of the manuscript.

FUNDING SOURCES

Research reported in this publication was supported by NIGMS of the National Institutes of Health under award number R35GM119623 to TRG.

REFERENCES

1 R. Booth and H. Kim, *Lab Chip*, 2012, **12**, 1784.
2 H. H. Chung, M. Mireles, B. J. Kwarta and T. R. Gaborski, *Lab Chip*, 2018, **18**, 1671–1689.
3 A. R. Mazzocchi, A. J. Man, J.-P. S. DesOrmeaux and T. R. Gaborski, *Cell. Mol. Bioeng.*, 2014, **7**, 369–378.
4 Z. Wang, S. H. Teoh, M. Hong, F. Luo, E. Y. Teo, J. K. Y. Chan and E. S. Thian, *ACS Appl. Mater. Interfaces*, 2015, **7**, 13445–13456.
5 V. Pensabene, L. Costa, A. Y. Terekhov, J. S. Gnecco, J. P. Wikswo and W. H. Hofmeister, *ACS Appl. Mater. Interfaces*, 2016, **8**, 22629–22636.
6 A. Granitzny, J. Knebel, M. Müller, A. Braun, P. Steinberg, C. Dasenbrock and T. Hansen, *Toxicol. reports*, 2017, **4**, 89–103.
7 S. J. Han, K. S. Bielawski, L. H. Ting, M. L. Rodriguez and N. J. Sniadecki, *Biophys. J.*, 2012, **103**, 640–648.
8 R. D. Sochol, A. T. Higa, R. R. R. Janairo, S. Li and L. Lin, *Soft Matter*, 2011, **7**, 4606.
9 R. D. Sochol, A. T. Higa, R. R. R. Janairo, S. Li and L. Lin, *Micro Nano Lett.*, 2011, **6**, 323.
10 S. Gholizadeh, Z. Allahyari, R. N. Carter, L. F. Delgadillo, M. Blaquiere, F. Nouguier-Morin, N. Marchi and T. R. Gaborski, *Adv. Mater. Technol.*, 2020, **5**, 2000474.
11 A. T. Salminen, Z. Allahyari, S. Gholizadeh, M. C. McCloskey, R. Ajalik, R. N. Cottle, T. R. Gaborski and J. L. McGrath, *Front. Med. Technol.*, 2020, 2, 11.
12 K. Kulangara and K. W. Leong, *Soft Matter*, 2009, **5**, 4072–4076.
13 J. M. Stukel and R. K. Willits, *Tissue Eng. - Part B Rev.*, 2016, 22, 173–182.

14 M. Ermis, E. Antmen and V. Hasirci, *Bioact. Mater.*, 2018, **3**, 355–369.
15 D. S. Hernandez, E. T. Ritschdorff, J. L. Connell and J. B. Shear, *J. Am. Chem. Soc.*, , DOI:10.1021/jacs.8b09226.
16 H. H. Chung, S. M. Casillo, S. J. Perry and T. R. Gaborski, *ACS Biomater. Sci. Eng.*, 2018, **4**, 222–230.
17 S. M. Casillo, A. P. Peredo, S. J. Perry, H. H. Chung and T. R. Gaborski, *ACS Biomater. Sci. Eng.*, 2017, **3**, 243–248.
18 Z. Allahyari, S. Gholizadeh, H. H. Chung, L. F. Delgadillo and T. R. Gaborski, *ACS Biomater. Sci. Eng.*, 2020, **6**, 959–968.
19 S. Dupont, L. Morsut, M. Aragona, E. Enzo, S. Giulitti, M. Cordenonsi, F. Zanconato, J. Le Digabel, M. Forcato and S. Bicciato, *Nature*, 2011, **474**, 179–183.
20 J. Byun, D. P. Del Re, P. Zhai, S. Ikeda, A. Shirakabe, W. Mizushima, S. Miyamoto, J. H. Brown and J. Sadoshima, *J. Biol. Chem.*, 2019, **294**, 3603–3617.
21 G. Nardone, J. Oliver-De La Cruz, J. Vrbsky, C. Martini, J. Pribyl, P. Skládal, M. Pešl, G. Caluori, S. Pagliari and F. Martino, *Nat. Commun.*, 2017, **8**, 1–13.
22 J.-H. Hwang, M. R. Byun, A. R. Kim, K. M. Kim, H. J. Cho, Y. H. Lee, J. Kim, M. G. Jeong, E. S. Hwang and J.-H. Hong, *PLoS One*, 2015, **10**, e0135519.
23 A. Nukuda, C. Sasaki, S. Ishihara, T. Mizutani, K. Nakamura, T. Ayabe, K. Kawabata and H. Haga, *Oncogenesis*, 2015, **4**, e165--e165.
24 V. A. Codelia, G. Sun and K. D. Irvine, *Curr. Biol.*, 2014, **24**, 2012–2017.
25 X. Qin, X. Lv, P. Li, R. Yang, Q. Xia, Y. Chen, Y. Peng, L. Li, S. Li and T. Li, *Biochim. Biophys. Acta (BBA)-Molecular Basis Dis.*, 2020, **1866**, 165625.
26 H. Pan, Y. Xie, Z. Zhang, K. Li, D. Hu, X. Zheng, Q. Fan and T. Tang, *Colloids Surfaces B Biointerfaces*, 2017, **152**, 344–353.
27 H. Ghasemi, S. H. Mousavibahar, M. Hashemnia, J. Karimi, I. Khodadadi, F. Mirzaei and H. Tavilani, *Ann. N. Y. Acad. Sci.*, 2020, **1473**, 48–61.
28 S. R. Caliari, S. L. Vega, M. Kwon, E. M. Soulas and J. A. Burdick, *Biomaterials*, 2016, **103**, 314–323.
29 D. M. Garcia Cruz, M. Gomes, R. L. Reis, D. Moratal, M. Salmerón-Sánchez, J. L. Gómez Ribelles and J. F. Mano, *J. Biomed. Mater. Res. Part A*, 2010, **95**, 1182–1193.
30 A. Cunha, O. F. Zouani, L. Plawinski, A. M. Botelho Do Rego, A. Almeida, R. Vilar and M. C. Durrieu, *Nanomedicine*, 2015, **10**, 725–739.
31 I. A. Paun, B. S. Calin, C. C. Mustaciosu, M. Mihailescu, C. S. Popovici and C. R. Luculescu, *J. Mater. Sci.*, 2019, **54**, 11213–11230.
32 D. Falconnet, D. Pasqui, S. Park, R. Eckert, H. Schift, J. Gobrecht, R. Barbucci and M. Textor, *Nano Lett.*, 2004, **4**, 1909–1914.
33 A. Azioune, N. Carpi, Q. Tseng, M. Théry and M. Piel, *Methods Cell Biol.*, 2010, **97**, 133–146.
34 B. D. Cosgrove, K. L. Mui, T. P. Driscoll, S. R. Caliari, K. D. Mehta, R. K. Assoian, J. A. Burdick and R. L. Mauck, *Nat. Mater.*, 2016, **15**, 1297–1306.
35 J. S. Park, J. S. Chu, A. D. Tsou, R. Diop, Z. Tang, A. Wang and S. Li, *Biomaterials*, 2011, **32**, 3921–3930.
36 P. Bandaru, G. Cefaloni, F. Vajhadin, K. Lee, H. Kim, H. Cho, M. C. Hartel, S. Zhang, W. Sun, M. J. Goudie, S. Ahadian, M. R. Dokmeci, J. Lee and A. Khademhosseini, *Small*, 2020, **16**, 2001837.
37 T. Yeung, P. C. Georges, L. A. Flanagan, B. Marg, M. Ortiz, M. Funaki, N. Zahir, W. Ming, V. Weaver and P. A. Janmey, *Cell Motil. Cytoskeleton*, 2005, **60**, 24–34.
38 E. A. Cavalcanti-Adam, A. Micoulet, J. Blümmel, J. Auernheimer, H. Kessler and J. P. Spatz, *Eur. J. Cell Biol.*, 2006, **85**, 219–224.
39 S. Tojkander, G. Gateva and P. Lappalainen, *J. Cell Sci.*, 2012, **125**, 1855–1864.
40 C. S. Chen, J. Tan and J. Tien, *Annu. Rev. Biomed. Eng.*, 2004, **6**, 275–302.
41 B. Wehrle-Haller, *Curr. Opin. Cell Biol.*, 2012, 24, 116–124.
42 K. Hayakawa, H. Tatsumi and M. Sokabe, *J. Cell Biol.*, 2011, **195**, 721–727.
43 J. Xia, Y. Yuan, H. Wu, Y. Huang and D. A. Weitz, *Biomaterials*, 2020, **248**, 120014.
44 R. N. Carter, S. M. Casillo, A. R. Mazzocchi, J.-P. S. DesOrmeaux, J. A. Roussie and T. R. Gaborski, *Biofabrication*, 2017, **9**, 015019.
45 A. Costa, C. de Souza Carvalho-Wodarz, V. Seabra, B. Sarmento and C. M. Lehr, *Acta Biomater.*, 2019, **91**, 235–247.
46 H. Cho, D. Kim and K. Kim, *Biotechnol. Bioprocess Eng.*, 2018, 23, 261–270.
47 M. Yan, L. Kluwe, R. E. Friedrich, X. Li, G. Ren, R. Smeets, M. Gosau and X. Liu, *Am. J. Transl. Res.*, 2020, **12**, 5781–5788.
48 M. Guvendiren and J. A. Burdick, *Biomaterials*, 2010, **31**, 6511–6518.
49 S. A. Ruiz and C. S. Chen, *Stem Cells*, 2008, **26**, 2921–2927.
50 R. Marom, I. Shur, R. Solomon and D. Benayahu, *J. Cell. Physiol.*, 2005, **202**, 41–48.
51 W. Zhao, X. Li, X. Liu, N. Zhang and X. Wen, *Mater. Sci. Eng. C*, 2014, **40**, 316–323.

SUPPLEMENTARY INFORMATION

METHODS AND MATERIALS

Generation of non-fouling micropattern on Silicon Dioxide (SiO_2)

SiO_2 substrates were fabricated and patterned using microfabrication techniques as previously reported.[1] Briefly, SiO_2 layer (300 nm) was deposited using plasma-enhanced chemical vapor deposition (PE-CVD) on a 150 mm single-side-polished silicon wafer. Upon applying MicroPrime MP-P20 as an adhesion promoter agent, Microposit S1813 photoresist was spin-coated, and soft-baked at 115 °C. This was followed by G-line exposure using GCA 6000-Series DSW 5X stepper to create 3 μm openings in the photoresist layer with hexagonally packed layout with 6 μm center-to-center spacing. The resist was developed with MF CD-26 developer and washed with DI water. The wafer was hard baked for 1 min at 150 °C. For development of non-fouling regions, 0.5 mg/ml of PLL(20)-g(3.5)-PEG(2) (Nanosoft Biotechnology LLC) in 10mM HEPES was placed on the substrates for 75 min. The optimum concentration and coating time were determined in an earlier work.[1] The substrates were washed twice immediately after removing PLL-g-PEG solution, followed by acetone wash to remove the photoresist and rinsed again with DI water. The non-fouling characteristic of the coated regions was confirmed by preventing protein adsorption and cell adhesion in an earlier study.[1] Silicone sheets were cut with pre-designed shapes with a digital craft cutter to obtain silicone gaskets for fabrication of cell culture devices. The chips were bonded to silicone gaskets using surface treatment with corona discharge using corona wand (Nbond, Littleton, CO) to restrain cell culture area.

Fabrication of ultrathin SiO2 membrane

Free-standing chip-supported SiO_2 membranes were fabricated using a combination of different microfabrication techniques as reported in our previous work.[2] Tetra-ethoxysilane (TEOS)-based PE-CVD was used to deposit a SiO_2 layer (300 nm) on both sides of a double-side-polished silicon wafer. The front-side was patterned with ASML PAS 5500/200 i-line stepper to obtain hexagonally packed 0.5 μm and 3 μm openings (1 μm and 6 μm center-center spacing, respectively), and it was thoroughly etched with reactive ion etching (RIE) using Drytek 482 Quad Etching tool. This was followed by annealing in nitrogen at 600 °C for film stress stabilization and increasing film robustness. The back-side SiO_2 layer was patterned and etched and the silicon wafer was etched with ethylenediamine pyrocatechol (EDP) to obtain final 5.4 mm × 5.4 mm square chips with 2 mm × 2 mm open windows, and the chips were cleaved for making individual chips. Similar to the non-fouling patterned substrates, silicone gaskets were fabricated and attached to the membranes to retain the cells on the membranes. The membranes were pre-treated with 0.15mg/ml solution of Geltrex which contains collagen IV, laminin and vitronectin for 30 min. Immunofluorescent staining was utilized to confirm the absence of fibronectin in the coated layer.

Cell culture

Adipose-derived stem cells (ADSCs) were purchased from ThermoFisher Scientific (Waltham, MA), and cultured in MesenPRO RS Medium with 2% Mesen-Pro Growth Supplement, 1% L- glutamine, and 1% Penicillin-Streptomycin. All the cell culture reagents were purchased from ThermoFisher Scientific unless stated otherwise. ADSCs were detached using TrypLE and seeded in the density of 2300 cells/cm for differentiation tests and 6000 cells/cm for the rest of the tests on all samples including non-fouling patterned SiO_2, porous membranes and control samples. ADSCs were used between passages 3-6.

Immunofluorescence

After 24 h of cell culture, the cells permeabilized using 0.1% Triton X-100 for 3 seconds, and fixed with 3.7% formaldehyde for 15 min. ADSCs were blocked with 2% (20 mg/ml) BSA for 15 min, and stained with DAPI (300 nM) for 3 min, 1:400 AlexaFluor 488 conjugated phalloidin for 15 min, and 1:100 eFluor570 conjugated anti-vinculin, Clone 759 for 2 h in room temperature to visualize nuclei, F-actins and focal adhesions, respectively. All the aforementioned steps followed by triple washing with PBS or DI water. For imaging the cells on non-fouling patterned substrates, the cells were washed and 10 μL PBS was placed to each sample. The samples were flipped on coverslips to enable imaging on them. However, for imaging on the porous membranes, the cells washed and the samples were only flooded with PBS without flipping since

it was only necessary for the non-transparent substrates. To visualize nuclei, F-actin and focal adhesions, the fluorescent images were acquired through DAPI, GFP and Texas red filters, respectively.

For YAP localization, ADSCs were fixed with 3.7% formaldehyde for 15 min, followed by permeabilizing with 0.1% Triton X-100 for 3 min. The cells were blocked with 4% (40 mg/ml) BSA for 15 min and stained with 1:100 AlexaFluor 488 conjugated YAP for 2 h to visualize YAP content. All the mentioned steps followed by triple PBS washing. The stained samples with AlexaFluor 488 conjugated YAP were imaged using GFP filter. All images were captured using Keyence BZ-X700 microscope (Keyence Corp. of America, MA) or Leica DMI6000 microscope (Leica Microsystems, Buffalo Grove, IL).

Actin intensity and focal adhesion analysis

The mean intensity of the actin fibers and the background intensity were determined from the actin cytoskeleton stained images in ImageJ software. This value multiplied by the spreading area of the cells to calculate the total F-actin content of each cell. Acquired fluorescent images of the stained cells with eFluor570 conjugated anti-vinculin were used to evaluate focal adhesions. Only cells with less than 10 percent cell-cell contact were analyzed. The number of distinct focal adhesions were counted for each cell.

Spreading Area analysis

The spreading area of the cells was obtained from the actin cytoskeleton stained images. The cell areas were calculated by identifying the perimeter of the cells manually using ImageJ software. DAPI images from nuclei confirmed each measured area belongs to a single cell, and the cell did not undergo mitosis.

YAP nuclear localization analysis

The fluorescent images of the stained cells using AlexaFluor 488 conjugated YAP were utilized to analyze YAP nuclear localization. The freehand selection tool of ImageJ software was used to measure the mean intensity value in the nucleus, in the cytoplasmic perinuclear region less than 10 um away from the nucleus, and in the background immediately adjacent to the cell. The background intensity was subtracted from the nuclear and cytoplasmic intensity values for each cell. In order to obtain the YAP nuclear localization ratio, the background-subtracted nuclear intensity was divided by the background-subtracted cytoplasmic intensity.

ADSC differentiation

ADSCs were seeded in the density of 2300 cell/cm2 on the 0.5 μm and 3 μm pores and nan-porous control SiO_2 in MesenPRO RS Medium. The MesenPRO RS Medium was removed, and a half and half mixture of adipogenic and osteogenic media with 1 % pen/strep were added to the samples after 24 h. ADSCs were cultured in this mixture for 10 days, and the media were changed every 3 days. ADSCs were fixed in 3.7% formaldehyde for 1 min and washed with DI water. The samples were stained for alkaline phosphatase and lipid vacuoles using Fast Blue RR and Oil Red O to evaluate their differentiation over each sample. Briefly, a pre-weighted capsule of fast blue RR was dissolved in 48 ml DI water, and 2 ml Naphthol was added to the solution. The solution was added to the fixed samples and washed twice with DI water after 30 min. Cells were incubated in 60% isopropanol, and the solution was removed after 5 min. Oil Red O working was prepared by adding 2 parts water to 3 parts 0.5 % Oil Red O in isopropanol. ADCSs were incubated in the Oil Red O working solution for 30 min and washed with DI water 4 times. The nuclei of ADSCs were stained using DAPI to assist with cell counting and calculating the percentage of the cells which went through osteogenic or adipogenic differentiation. Brightfield images were captured from each sample to visualize their lipid vacuoles and alkaline phosphatase. The differentiation on each sample was calculated using the overlap of the brightfield and DAPI fluorescent images.